Guilong Li
State Key Laboratory of Mechanical System and Vibration, Shanghai Jiaotong University, Shanghai 200240, China; School of Mechanical Engineering, Shanghai Jiaotong University, Shanghai 200240, China
e-mail: lgl52613@sjtu.edu.cn

Shichang Du[1]
State Key Laboratory of Mechanical System and Vibration, Shanghai Jiaotong University, Shanghai 200240, China; School of Mechanical Engineering, Shanghai Jiaotong University, Shanghai 200240, China
e-mail: lovbin@sjtu.edu.cn

Delin Huang
State Key Laboratory of Mechanical System and Vibration, Shanghai Jiaotong University, Shanghai 200240, China; School of Mechanical Engineering, Shanghai Jiaotong University, Shanghai 200240, China
e-mail: cjwanan@sjtu.edu.cn

Chen Zhao
State Key Laboratory of Mechanical System and Vibration, Shanghai Jiaotong University, Shanghai 200240, China; School of Mechanical Engineering, Shanghai Jiaotong University, Shanghai 200240, China
e-mail: zhao_chen@sjtu.edu.cn

Yafei Deng
State Key Laboratory of Mechanical System and Vibration, Shanghai Jiaotong University, Shanghai 200240, China; School of Mechanical Engineering, Shanghai Jiaotong University, Shanghai 200240, China
e-mail: phoenixdyf@sjtu.edu.cn

Dynamics Modeling-Based Optimization of Process Parameters in Face Milling of Workpieces With Discontinuous Surfaces

Face milling is widely used in machining processes, aimed at providing workpieces with high surface quality. The chatter generated in face milling could lead to tremendous damage to machine tools, poor machined surface quality, and loss of processing efficiency. Most related researches have been focused on the modeling of spindle dynamics and discretization algorithms for chatter prediction. However, few published articles have taken the geometric characteristics of workpieces into consideration, especially for workpieces with discontinuous surfaces in face milling, which leads to poor accuracy of chatter prediction as well as the waste of processing efficiency. To overcome this shortage, a novel dynamic model for the face milling process is built in this paper, considering the cutting insert engagement based on the geometric characteristics of the workpieces and the tool path. The stability lobe diagrams (SLDs) applicable to workpieces with discontinuous surfaces are constructed. A process parameter optimization model is developed to maximize the chatter-free processing efficiency of the face milling process. The sensitivity analysis is utilized to simplify the objective function, and the genetic algorithm is employed to solve the optimization model. The proposed approach is validated by an experimental case study of an engine block, improving the chatter-free material removal rate by 53.3% in comparison to the classic approach. [DOI: 10.1115/1.4044421]

Keywords: dynamics modeling, face milling, discontinuous surfaces, chatter prediction, process parameter optimization, machine tool dynamics, machining processes

1 Introduction

Due to the high-processing efficiency and the machining quality, face milling is commonly implemented in industries such as automobile, shipbuilding, and aerospace [1–3]. The regenerative chatter induced by unsuitable process parameters in face milling is still a primary obstacle that limits the further improvement of processing efficiency [4,5] machined surface quality [6,7], and the prolongation of tool lifetime [8,9].

To obtain a better understanding of the physical mechanism of chatter phenomenon, scholars have been working on dynamics modeling and chatter prediction for years. Since Tobias [10] and Tlusty [11] laid the foundation of the classic chatter theories, methodologies for dynamics modeling and chatter prediction have been developed continuously, including analytical, numerical, and experimental ones. Sridhar et al. [12] developed an analytical model to describe the dynamic behavior of the general milling process, and this model was solved by a numerical method. Zheng et al. [13] proposed an analytical method to determine the worst spindle speeds and the critical limiting axial depth of cut for a two-degree-of-freedom (2-DOF) milling system of planar isotropic dynamics. Minis et al. [14,15] proposed theoretical approaches for prediction of linear and nonlinear chatter in the milling process. By using Timoshenko beam theory to obtain the frequency response of the machining system, Movahhedy and Mosaddegh [16] built a finite element based model including the gyroscopic effects to predict chatter in high-speed milling. Ding et al. [17] proposed a full-discretization method for prediction of milling stability,

[1]Corresponding author.
Manuscript received May 14, 2019; final manuscript received July 23, 2019; published online August 2, 2019. Assoc. Editor: Tony Schmitz.

which is derived based on the direct integration scheme. Li et al. [18] proposed a Runge-Kutta-based complete discretization method to predict the chatter stability of the milling process. Based on the studies by Ding et al. [17] and Li et al. [18], Dai et al. [19] adopted the explicit precise integration method (PIM) to improve the convergence rate and prediction accuracy. Ismail and Soliman [20] proposed an experimental method for quick identification of the stability lobes in the milling process by monitoring the response of a chatter indicator and ramping the spindle speed simultaneously. Lee and Park [21] developed a capsule-type modular machine tool to deal with multifunctional processes with a single setup, and the dynamic behavior of the machine tool was verified by an experimental frequency response function (FRF) test and a FRF simulation. By utilizing substructuring and perturbation methods, Tuysuz and Altintas [22] proposed a new reduced-order time-domain model, which is four times more computationally efficient than their previously proposed frequency-domain model [23].

As one of the most effective and efficient methods of chatter prediction, the stability lobe diagram (SLD) has received continuous concern from researchers. Smith and Tlusty [24] proposed an algorithm to generate stability lobes in the milling process by time-domain simulations. Cao et al. [25] proposed an alternative approach to establish the SLD of high-speed milling considering speed-varying spindle dynamics. Quintana et al. [26] applied the sound mapping methodology to determine the SLD of a milling process. Altintas and Budak [27] utilized the zero-order analytical (ZOA) method to predict the chatter stability lobes for the milling process. Merdol and Altintas [28] expanded the ZOA method and presented the multifrequency method to improve the transfer function with the harmonics of the tooth passing frequencies. By expanding the dynamics modeling of Budak and Altintas to a three-dimensional case, Jensen and Shin [29,30] developed an algorithm to predict stability lobes in face milling operation based on frequency-domain analysis. More recently, by considering the joint influences of cutting parameters, tool geometries, and runout, Niu et al. [31] studied the patterns of regenerative chatter in general milling scenarios. Caliskan et al. [32] proposed a novel on-line chatter detection method by monitoring the vibration energy. Tang et al. [33] presented a new stability analysis method to analyze the effect of tool orientation on machining efficiency for five-axis bull-nose end milling.

Based on the dynamics modeling and chatter prediction, the optimization of process parameters is the next topic that has aroused the interest of scholars. Baek et al. [34] analyzed the effects of the insert runout errors and the variation of the feed rate on the surface roughness and the dimensional accuracy in a face-milling operation using a surface roughness model. An optimization model of the feed rate was developed, aimed at maximizing material removal rate under the given surface roughness constraint. Song et al. [35] proposed an optimization method of cutting parameters considering the self-excited and forced vibrations in peripheral milling processes. Zhang and Ding [36] developed the procedures of optimization of machining parameters in the chatter-free milling process. Furthermore, by considering the uncertainties of dynamics of the milling system [37] and interference-free between tool and flexible workpiece [38], Zhang et al. have proposed corresponding optimization models of process parameters.

These researches reviewed above could provide reasonable dynamics modeling, chatter prediction, and parameter optimization for most general milling processes of workpieces with continuous surfaces; yet, the cases of workpieces with discontinuous surfaces are almost neglected in the literature. Since the dynamic cutting forces are definitely dependent on the tool path and the material distribution of the workpiece [39–41], the exact interaction between the disc milling cutter and the workpiece should be taken into consideration for a more accurate chatter prediction in face milling. In order to obtain a more accurate estimation of the dynamic cutting forces, workpiece characteristics should be taken into consideration, such as the physical structure and continuity of the machined surface. However, conventional models are mainly focused on workpieces with continuous surfaces, which will lead to an inaccurate prediction of chatter stability when facing to workpieces with discontinuous surfaces. With the rapid development of manufacturing industry, physical structures of workpieces have been increasingly complex [42–44]. For instance, a four-cylinder engine block as depicted in Fig. 1, made of gray cast iron HT250, is a typical workpiece with discontinuous surfaces. There are four-cylinder bores distributed along the midline of the top surface of the engine block with an equal interval between each other. Besides, there are several minor holes used for assembly positioning, installing bolts, and circulating water or oil. All of these cylinder bores and minor holes have aggravated the complexity of workpiece geometry as well as the stiffness distribution of the workpiece. It is a challenge to accurately express the dynamics during the face milling on the top surface of an engine block, due to the tremendous change in the workpiece geometry [45]. Without a suitable and reliable dynamic cutting force model for chatter prediction, the optimization of process parameters is hard to implement for the face milling process of workpieces with discontinuous surfaces.

However, the detailed and easily applicable optimization algorithm taking the face milling mechanism into account is absent to date. Zhang et al. [46] proposed a Taguchi design application to optimize surface quality in a computer numerical control (CNC) face milling operation. Based on the Taguchi method, Asiltürk and Neseli [47] utilized response surface analysis (RSA) to determine multi-objective optimal cutting conditions in a CNC turning process. Mhapsekar et al. [48] proposed the manufacturing constraints integrated with the density-based topology optimization algorithm for additive manufacturing. Lu et al. [49] proposed an optimization model of the cutting parameters in high-speed end milling on SKD61 tool steel, utilizing grey relational analysis coupled with principal component analysis to solve the model. Using genetic algorithm (GA), Pang and Kishawy [50] introduced an inverse analysis on the primary shear zone to determine the five constants in Johnson-Cook's material constitutive equation under the conditions of metal cutting. Most researches related to process parameter optimization are focused on the heuristic or statistical optimization algorithm itself, regardless of the physical model of the machining process. Especially, there is a lack of appropriate physical models for face milling process of workpieces with discontinuous surfaces, leading to inaccurate chatter prediction and misguided choice of process parameters. To this end, a dynamics modeling-based analytical approach is proposed in this paper to maximize the chatter-free processing efficiency by optimizing the processing parameters for the face milling process of workpieces with discontinuous surfaces. The effect of the cutter-workpiece interaction is embodied in the determination of the dynamic number of inserts engaged with the workpiece during the cutting process, which is termed as cutting insert engagement.

The main contribution of this paper lies in proposing an analytical process parameter optimization method, considering the effect of cutting insert engagement on dynamics modeling of the face milling system, which is mathematically derived based on the

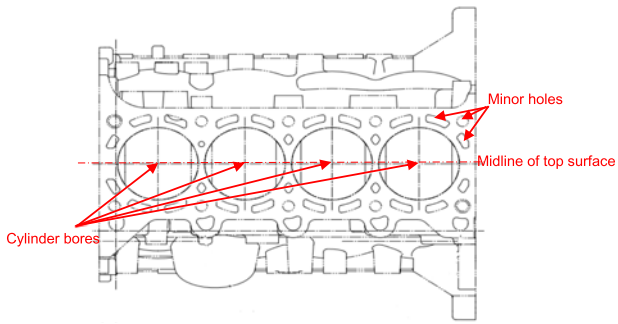

Fig. 1 Top view of a four-cylinder engine block

geometric characteristics of the disc milling cutter and the workpiece with the discontinuous surface.

The remainder of the paper is organized as follows. Section 2 shows the specific procedures of the proposed approach, including dynamic cutting force modeling, determination of cutting insert engagement, chatter stability prediction, sensitivity analysis, and optimization of process parameters. In Sec. 3, the effectiveness of the proposed approach is demonstrated by a machining experiment on a type of four-cylinder engine block, and the comparison of experimental results between the proposed approach and the classic approach [29] is given. Section 4 is devoted to the conclusion of this study.

2 The Proposed Approach

2.1 Dynamic Cutting Force Modeling. Without loss of generality, the face milling system can be simplified to a 2-DOF vibration system [11,51] as shown in Fig. 2. Therein, two spring damping subsystems are employed to generate vibrations along *X*-axis and *Y*-axis, respectively, and θ_{st} is the starting angle while θ_{ex} is the exiting angle. Supposing that there are a total of N_c inserts on the disc milling cutter and the cutting edge of each insert is divided into M microelements, for the *l*th microelement of the cutting edge of *j*th insert engaged with the workpiece, the radial immersion angle is denoted as

$$\theta_{j,l} = \theta_{1,0} + \frac{2\pi(j-1)}{N_c} + \frac{a_p l \tan\beta}{MR_c} \tag{1}$$

where $\theta_{1,0}$, a_p, β, and R_c denote angular displacement of the bottom of the first cutting edge, axial cutting depth, angle of the flank edge, and ideal radius of the disc milling cutter, respectively, for $j = 1, 2,\ldots, N_c$ and $l = 1, 2,\ldots, M$.

In this simplified 2-DOF face milling model, the cutting forces are projected in two orthogonal directions, denoted by F_x and F_y, respectively, which can be formulated as

$$\begin{cases} m_x\ddot{x}(t) + c_x\dot{x}(t) + k_x x(t) = F_x(t) \\ m_y\ddot{y}(t) + c_y\dot{y}(t) + k_y y(t) = F_y(t) \end{cases} \tag{2}$$

where m_x, m_y, c_x, c_y, k_x, and k_y are the mass, damping, and stiffness of the cutter-workpiece system along *X*-axis and *Y*-axis, respectively.

As shown in Fig. 3, the cutting force on one of the microelements of a cutting edge *dF* can be decomposed into three mutually perpendicular components, i.e., the axial, radial, and tangential force denoted by dF_a, dF_r, and dF_t, respectively. These components are transformed into the machine coordinate system and represented as

$$\begin{cases} dF_{x,j,l} = -dF_{t,j,l}\cos\theta_{j,l} - dF_{r,j,l}\sin\theta_{j,l} \\ dF_{y,j,l} = -dF_{t,j,l}\sin\theta_{j,l} - dF_{r,j,l}\cos\theta_{j,l} \\ dF_{z,j,l} = dF_{a,j,l} \end{cases} \tag{3}$$

Considering the actual interaction between the disc milling cutter and the workpiece, the cutting forces are generated on the cutting edges of inserts engaged with the workpiece, whereas those on the rest of inserts are set to zero. Note that the number of inserts engaged with the workpiece, denoted by N, is a time-varying parameter, which will be determined in Sec. 2.2. Superimposing the force components on all cutting edges engaged in material removal at a certain moment, yields

$$\begin{cases} F_x = \sum_{j=1}^{N}\sum_{l=1}^{M}[-dF_{t,j,l}\cos\theta_{j,l} - dF_{r,j,l}\sin\theta_{j,l}] \\ F_y = \sum_{j=1}^{N}\sum_{l=1}^{M}[dF_{t,j,l}\sin\theta_{j,l} - dF_{r,j,l}\cos\theta_{j,l}] \\ F_z = \sum_{j=1}^{N}\sum_{l=1}^{M} dF_{a,j,l} \end{cases} \tag{4}$$

For the exponential instantaneous model [52,53], during each revolution of the disc milling cutter, the average cutting force

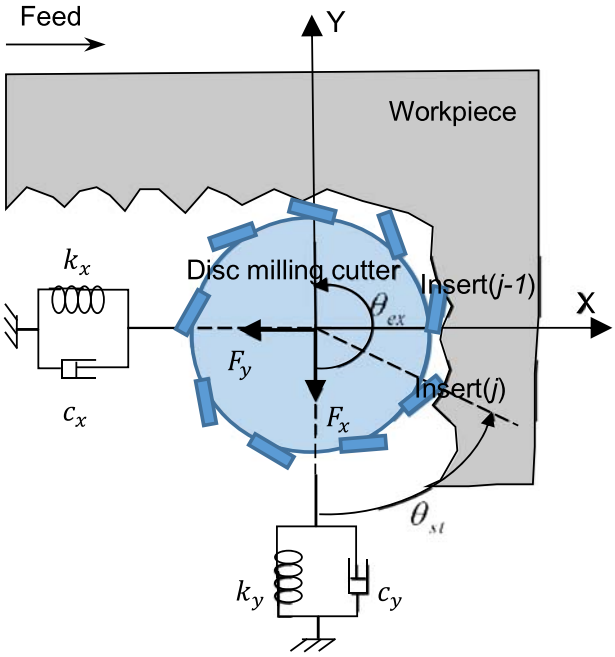

Fig. 2 The simplified 2-DOF face milling model

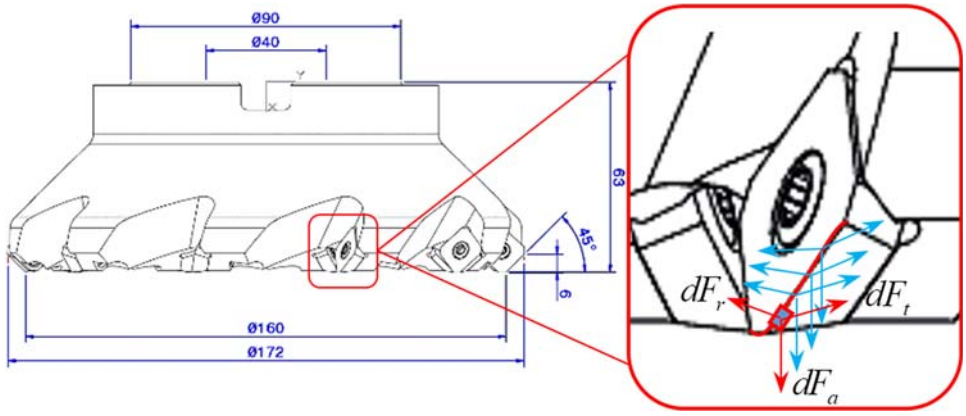

Fig. 3 Milling force components on the cutting edge of an insert

components along each axis can be calculated by Eq. (5), respectively,

$$\begin{cases} F_{A,x} = \dfrac{a_p N}{2\pi} K_t f_z^{A_x} \displaystyle\int_{\theta_{st}}^{\theta_{ex}} (\sin\theta)^{1-A_x}\, d\theta \\ F_{A,y} = \dfrac{a_p N}{2\pi} K_t f_z^{A_y} \displaystyle\int_{\theta_{st}}^{\theta_{ex}} (\sin\theta)^{1-A_y}\, d\theta \\ F_{A,z} = \dfrac{a_p N}{2\pi} K_a f_z^{A_z} \displaystyle\int_{\theta_{st}}^{\theta_{ex}} (\sin\theta)^{A_z}\, d\theta \end{cases} \tag{5}$$

Therein, K_r, K_t, and K_a denote the radial, tangential, and axial cutting coefficients, respectively, given by

$$\begin{cases} K_r = \dfrac{2\pi e^{B_x}}{\int_{\theta_{st}}^{\theta_{ex}} (\sin\theta)^{1+A_x} d\theta} \\ K_t = \dfrac{2\pi e^{B_y}}{\int_{\theta_{st}}^{\theta_{ex}} (\sin\theta)^{1+A_y} d\theta} \\ K_a = \dfrac{2\pi e^{B_z}}{\int_{\theta_{st}}^{\theta_{ex}} (\sin\theta)^{A_z} d\theta} \end{cases} \tag{6}$$

and f_z refers to the feed per insert.

Taking the logarithm on both sides of Eq. (5) yields

$$\ln\left(\frac{F_{A,q}}{a_p N}\right) = A_q \ln f_z + B_q \tag{7}$$

where A_q and B_q (for $q = x, y, z$) are pending coefficients substituting K_r, K_t, and K_a. Since Eq. (7) is obviously a group of linear equations, both A_q and B_q can be obtained by the least square method through multiple sets of experimental tests of cutting forces using different process parameters. Thus, the average cutting force components along each axis can be calculated by Eq. (7), respectively.

Denoting the regeneration displacement vector at an arbitrary moment t as $\{\Delta(t)\}$, the dynamic cutting force model can be formulated as

$$\{F(t)\} = \frac{1}{2} a_p K_t [A(t)] \{\Delta(t)\} \tag{8}$$

where $A(t)$ is the directional coefficient matrix which is a periodic function varying with time and the radial immersion angle of the milling cutter. The angular frequency of $A(t)$ is $\omega = \frac{\Omega N_c}{60}$.

Using the matrix form, Eq. (8) can be further expressed as

$$\begin{Bmatrix} F_x \\ F_y \end{Bmatrix} = \frac{1}{2} a_p K_t \begin{bmatrix} a_{xx} & a_{xy} \\ a_{yx} & a_{yy} \end{bmatrix} \begin{Bmatrix} \Delta x \\ \Delta y \end{Bmatrix} \tag{9}$$

where a_{xx}, a_{xy}, a_{yx}, and a_{yy} are the directional coefficients.

In order to remove the time dependency of $A(t)$, the directional coefficients are expanded into Fourier series and averaged separately. Since Budak and Altintas [54,55] proved that higher-order harmonics of periodic functions do not affect prediction accuracy, by preserving only the zero-order term of the Fourier series, the time-invariant directional coefficient matrix $[A_0]$ can be obtained as follows:

$$[A_0] = \frac{N}{2\pi} \begin{bmatrix} \alpha_{xx} & \alpha_{xy} \\ \alpha_{yx} & \alpha_{yy} \end{bmatrix} \begin{Bmatrix} \Delta x \\ \Delta y \end{Bmatrix} \tag{10}$$

where a_{xx}, a_{xy}, a_{yx}, and a_{yy} are termed as the average directional coefficients and given by

$$\begin{cases} \alpha_{xx} = 2\int_{\theta_{st}}^{\theta_{ex}} (\sin 2\theta + K_r(1 - \cos 2\theta)) d\theta \\ \alpha_{xy} = 2\int_{\theta_{st}}^{\theta_{ex}} (1 + \cos 2\theta + K_r \sin 2\theta) d\theta \\ \alpha_{yx} = 2\int_{\theta_{st}}^{\theta_{ex}} (-1 + \cos 2\theta + K_r \sin 2\theta) d\theta \\ \alpha_{yy} = 2\int_{\theta_{st}}^{\theta_{ex}} (-\sin 2\theta + K_r(1 + \cos 2\theta)) d\theta \end{cases} \tag{11}$$

Therefore, the dynamic cutting force model for the face milling process can be rewritten as

$$\{F(t)\} = \frac{N a_p}{4\pi} K_t \boldsymbol{\alpha} \{\Delta(t)\} \tag{12}$$

Therein, $\boldsymbol{\alpha}$ is independent of time and only varying with the radial immersion angle.

2.2 Determination of Cutting Insert Engagement. In general, the chatter observed in a face milling operation is mainly induced by the regenerative effect and closely coupled to the dynamic cutting forces. As the cutting inserts are engaged with the workpiece, the dynamic cutting forces and undulations are periodically generated during the mutual extrusion and friction between the inserts and workpiece for every revolution. The cutter-workpiece vibrations are sustained by the undulations generated in the previous revolution of the disc milling cutter, which is termed as the regenerative effect. As for workpieces with the simple physical structure and continuous material distribution, the face milling process is continual and the cutting insert engagement is smooth and steady thus almost neglected in the existing literature. However, as for workpieces with discontinuous surfaces and complex physical structure (such as multiple holes and chambers), the cutting insert engagement is dependent on the cutting path and the workpiece characteristics, which makes the regenerative process relatively irregular. The dynamic cutting force model formulated by Eq. (12) is a function of N. Hence, neglect of the effect of cutting insert engagement is unsuitable for workpieces with discontinuous surfaces and might eventually lead to an inaccurate prediction of chatter stability.

In order to obtain a suitable dynamic cutting force model for workpieces with discontinuous surfaces, this section is devoted to the determination of cutting insert engagement, taking the face milling process of a typical workpiece with multiple cylindrical bores as an instance. Figure 4 exhibits how the cutting insert engagement (i.e., N) varies along the feed direction. Since the diameter of the disc milling cutter D_c is larger than the radial cutting depth a_e, the face milling process is intermittent. Moreover, due to the material distribution, N decreases when the disc milling cutter reaches the cylindrical bores and vice versa. In summary, the variation pattern of N is complex yet computable.

Before the determination of cutting insert engagement, several definitions of parameters used in the derivation process are introduced in Table 1.

Based on these definitions, there are two important and reasonable hypotheses proposed in this paper.

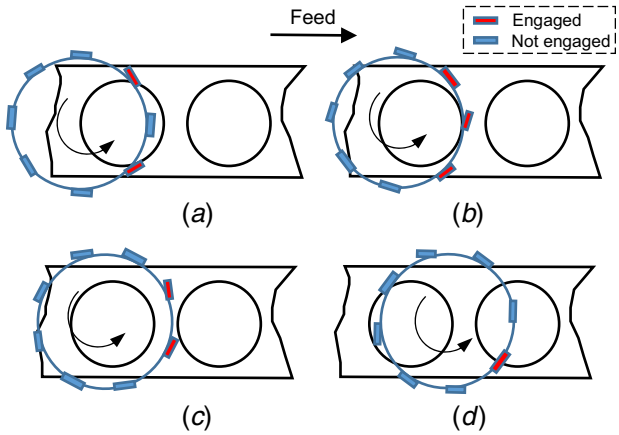

Fig. 4 Variation of cutting insert engagement along the feed direction: (*a*) *N* = 2, (*b*) *N* switches from 2 to 3, (*c*) *N* switches from 3 to 2, and (*d*) *N* switches from 2 to 1

Table 1 Definitions of parameters used in the derivation process

Parameter	Definition	Function
Cutting duration (s)	$t_c = t_{now} - t_0$	Duration from the start of cutting (t_0) to observation (t_{now})
Cutting distance (m)	$L_c = V_f t_c$	Maximum distance between edges of cutter and workpiece along feed direction
Cutting speed (m/s)	$V_c = \frac{\pi D_c \Omega}{60}$	Linear velocity of each insert
Micro element of cutting distance (m)	$\Delta L_c = V_f \frac{\pi D_c}{V_c}$	Feed per revolution of the disc milling cutter

Hypothesis I: The face milling process of the typical workpiece with discontinuous surfaces is finished by a disc milling cutter within a single pass from the front face to the rear face, and the cutting path passes through all centers of the cylindrical bores, i.e., the cutting path coincides with the midline of the top surface. This hypothesis is almost in line with the actual manufacturing process and convenient for the subsequent mathematical deduction.

Hypothesis II: The cutting speed V_c is far greater than the feed rate V_f and the feed per revolution (denoted by ΔL_c) is quite small, which can be regarded as a microelement of L_c. During each revolution, the change of N depends only on the length of the cutting arc, as shown in Fig. 5. L_k and L_{k+1} (for $k = 1, 3, 5, 7$) are the horizontal distances from the front face to the nearest and the farthest generatrix of the $(k/2 + 1/2)$th cylindrical bore, respectively. The length of cutting arc is a single-variable function of L_c and closely related to the geometric characteristics of the workpiece. Based on the length of the cutting arc, the whole face milling process can be divided into several phases. For each phase of cutting, the cutting insert engagement can be determined by establishing the piecewise function for the length of the cutting arc.

Denoting the radius of a cylindrical bore, the length and width of a typical workpiece by R_b, L_a, and L_b, respectively, the cutting insert engagement can be determined phase by phase and the illustrations for each phase are summarized in Fig. 6.

Phase I: After the edge of the disc milling cutter reaches the front face, the cutting forces start to be generated by the interaction between the cutter and workpiece. And the face milling process enters *phase I*, which is defined by $0 \le L_c \le L_1$. The radial cutting depth a_e is given by

$$a_e = \sqrt{D_c^2 - (D_c - 2L_c)^2} \tag{13}$$

Of note is that there are two possible circumstances that need to be discussed separately. Dependent on the dimensions of the disc milling cutter and the machined engine block, a special phase termed as *phase I** might emerges before the face milling process enters *phase II*.

(i) Under the circumstance of $\sqrt{D_c^2 - (D_c - 2L_1)^2} \le L_b$, as depicted in Fig. 6(*a*), the length of cutting arc is continuously increasing during the whole duration of *phase I*. This circumstance is deemed as the "normal" one due to the continuous change of the length function of the cutting arc. For every single revolution of the disc milling cutter, the number of inserts engaged with the workpiece N is proportional to the length of cutting arc. Therefore, the cutting insert engagement of *phase I* can be formulated as

$$N = \frac{N_c}{\pi} \arccos \frac{D_c - 2L_c}{D_c} \tag{14}$$

(ii) Under the circumstance of $\sqrt{D_c^2 - (D_c - 2L_1)^2} > L_b$, as depicted in Fig. 6(*b*), *phase I* is immediately followed by *phase I**. As the face milling proceeds, a_e grows from 0 to L_b; however, the disc milling cutter is still away from the first cylindrical bore. This circumstance is induced by the oversized D_c and the skimpy L_1. Before the face milling process enters *phase II*, the length of cutting arc is a constant during the whole duration of *phase I**. And the cutting insert engagement considering the emergence of *phase I** can be calculated by

$$N = \begin{cases} \frac{N_c}{\pi} \arccos \frac{D_c - 2L_c}{D_c} & 0 \le L_c \le \frac{D_c - \sqrt{D_c^2 - L_b^2}}{2} \\ \frac{N_c}{\pi} \arcsin \frac{L_b}{D_c} & \frac{D_c - \sqrt{D_c^2 - L_b^2}}{2} < L_c \le L_1 \end{cases} \tag{15}$$

Phase II: Once the disc milling cutter reaches the first cylindrical bore, the face milling process starts to enter *phase II*, which is defined by $L_1 \le L_c \le L_2$. The cutting arc is segmented into two symmetrical pieces due to the material vacancy of the cylindrical bore. The total length of the cutting arcs decreases first and then increases. Similar to the cutting insert engagement of *phase I*, there are two possible circumstances needing separate discussion as well.

(i) Under the circumstance of $\sqrt{D_c^2 - (D_c - 2L_1)^2} < L_b$, *phase II** emerges (see Fig. 6(*c*)). Note that the criterion for *phase II** is not exactly the same as that for *phase I*, because both *phase I** and *phase II** will make no sense if $\sqrt{D_c^2 - (D_c - 2L_1)^2}$ is just equivalent to L_b. Besides, *phase I** and *phase II** will not emerge in the same face milling case, and it is possible that neither of these two special phases emerges in the entire face milling process. The cutting insert engagement considering the emergence of *phase II** can be formulated as

$$N = \begin{cases} \frac{N_c}{\pi} \left(\arccos \frac{D_c - 2L_c}{D_c} - \arccos \frac{4S_{t1}}{D_c L_{y1}} \right) & L_1 \le L_c \le \frac{D_c - \sqrt{D_c^2 - L_b^2}}{2} \\ \frac{N_c}{\pi} \left(\arcsin \frac{L_b}{D_c} - \arccos \frac{4S_{t1}}{D_c L_{y1}} \right) & \frac{D_c - \sqrt{D_c^2 - L_b^2}}{2} < L_c \le L_2 \end{cases} \tag{16}$$

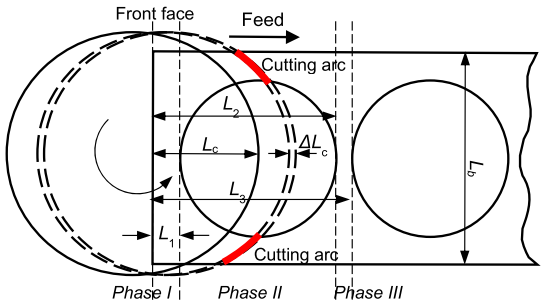

Fig. 5 Phase division based on the cutting arc

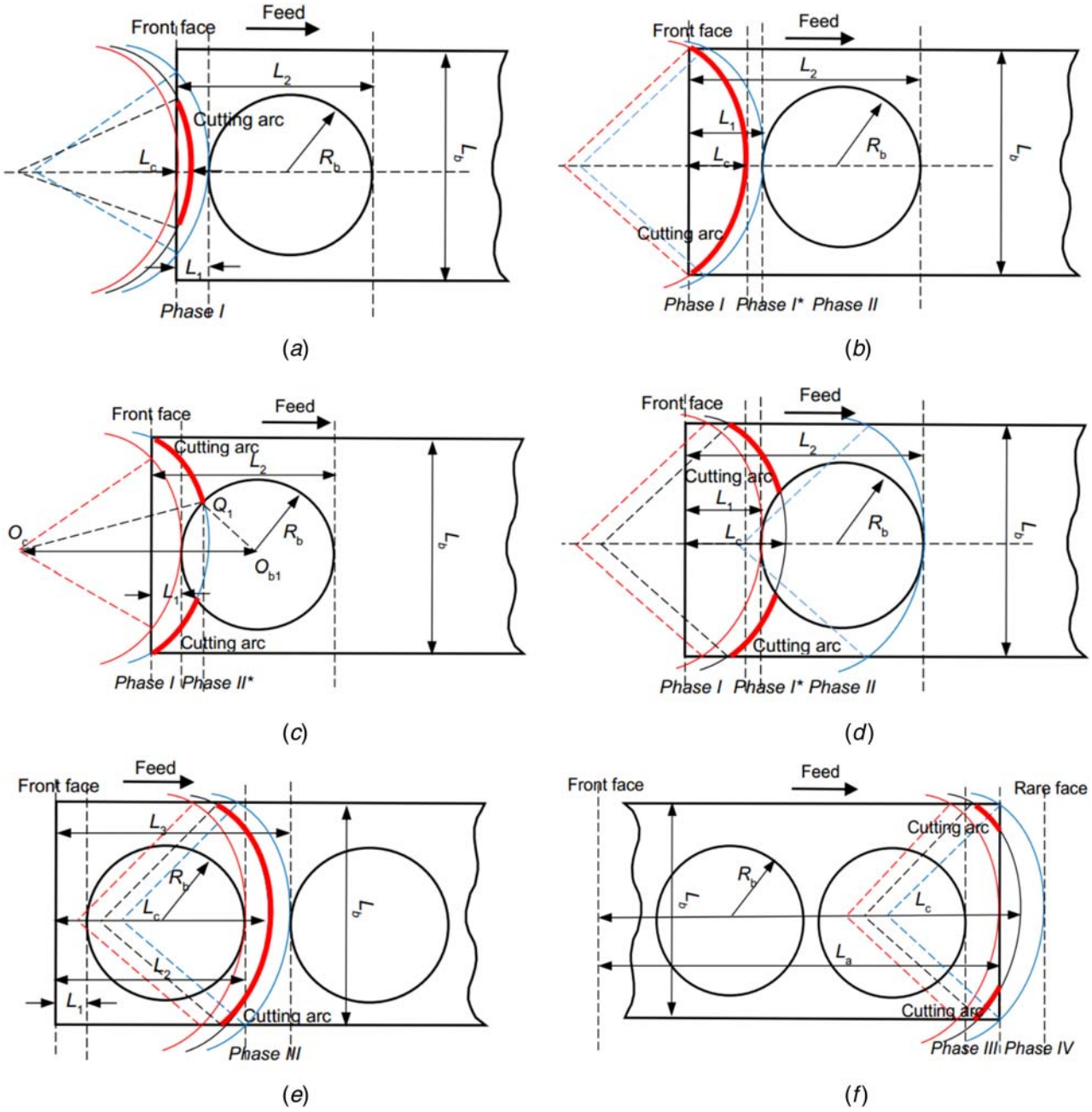

Fig. 6 Cutting insert engagement for different phases: (*a*) *phase I* without the emergence of *phase I, (*b*) *phase I* with the emergence of *phase I**, (c) *phase II* with the emergence of *phase II**, (*d*) *phase II* without the emergence of *phase II**, (e) *phase III*, and (*f*) *phase IV***

Therein, L_{y1} is the distance between the centers of the disc milling cutter and the first cylindrical bore and S_{t1} is the area of the triangular $Q_1O_cO_b$ which can be calculated by the Heron's Formula [56]. The detailed derivation can be found in the Appendix.

(1) Under the circumstance of $\sqrt{D_c^2-(D_c-2L_1)^2} \geq L_b$, the radial cutting depth a_e has already been equal to the width of the engine block L_b before the disc milling cutter reaches the first cylindrical bore (see Fig. 6(*d*)). The cutting insert engagement of *phase II* can be formulated as

$$N=\frac{N_c}{\pi}\left(\arcsin\frac{L_b}{D_c}-\arccos\frac{4S_{t1}}{D_cL_{y1}}\right) \tag{17}$$

Phase III: This phase is defined by $L_2 \leq L_c \leq L_3$, where two separate cutting arcs are combined again to form a single cutting arc (see Fig. 6(*e*)). And the length of cutting arc remains constant during the whole of *phase III* given as

$$N=\frac{N_c}{\pi}\arcsin\frac{L_b}{D_c} \tag{18}$$

Phase IV: Subsequently, the face milling process will enter *phase II* and *phase III* for several cycles, not reiterated here, until the last cylindrical bore is passed through completely, and the face milling process eventually enters *phase IV* (see Fig. 6(*f*)). *Phase IV* is defined by $L_a \leq L_c \leq L_a + ((D_c - \sqrt{D_c^2 - L_b^2})/2)$ and deemed as the final phase of the face milling process. The disc milling cutter starts to leave the top surface of the workpiece. The cutting arc length is segmented into two symmetrical pieces again and continuously decreases to 0. The cutting insert engagement of

Table 2 Formulas of cutting insert engagement *N* for different phases

Phase	Formula of cutting insert engagement	In case of
I ($0 \le L_c \le L_1$)	$N = \frac{N_c}{\pi}\arccos\frac{D_c - 2L_c}{D_c}$	$\sqrt{D_c^2 - (D_c - 2L_1)^2} \le L_b$
	$\begin{cases} \frac{N_c}{\pi}\arccos\frac{D_c - 2L_c}{D_c} & \left(0 \le L_c \le \frac{D_c - \sqrt{D_c^2 - L_b^2}}{2}\right) \\ \frac{N_c}{\pi}\arcsin\frac{L_b}{D_c} & \left(\frac{D_c - \sqrt{D_c^2 - L_b^2}}{2} < L_c \le L_1\right) \end{cases}$	$\sqrt{D_c^2 - (D_c - 2L_1)^2} > L_b$
II ($L_1 \le L_c \le L_2$)	$\begin{cases} \frac{N_c}{\pi}\left(\arccos\frac{D_c - 2L_c}{D_c} - \arccos\frac{4S_{t1}}{D_c L_{y1}}\right) & \left(L_1 \le L_c \le \frac{D_c - \sqrt{D_c^2 - L_b^2}}{2}\right) \\ \frac{N_c}{\pi}\left(\arcsin\frac{L_b}{D_c} - \arccos\frac{4S_{t1}}{D_c L_{y1}}\right) & \left(\frac{D_c - \sqrt{D_c^2 - L_b^2}}{2} < L_c \le L_2\right) \end{cases}$	$\sqrt{D_c^2 - (D_c - 2L_1)^2} < L_b$
	$\frac{N_c}{\pi}\left(\arcsin\frac{L_b}{D_c} - \arccos\frac{4S_{t1}}{D_c L_{y1}}\right)$	$\sqrt{D_c^2 - (D_c - 2L_1)^2} \ge L_b$
III ($L_2 \le L_c \le L_3$)	$\frac{N_c}{\pi}\arcsin\frac{L_b}{D_c}$	—
IV $\left(L_a \le L_c \le L_a + \frac{D_c - \sqrt{D_c^2 - L_b^2}}{2}\right)$	$N = \frac{N_c}{\pi}\left(\arcsin\frac{L_b}{D_c} - \arccos\frac{D_c - 2L_c + 2L_a}{D_c}\right)$	—

phase IV can be formulated as

$$N = \frac{N_c}{\pi}\left(\arcsin\frac{L_b}{D_c} - \arccos\frac{D_c - 2L_c + 2L_a}{D_c}\right) \tag{19}$$

To facilitate comparative reading, the mathematical formulas of cutting insert engagement N for different phases are summarized in Table 2.

As shown in Fig. 7, there are three possible cases for the face milling process, dependent on the diameter of the disc milling cutter as well as the geometric characteristics of the workpiece.

In summary, the phase division-based determination of cutting insert engagement makes significance for the dynamic cutting force and milling chatter prediction with higher accuracy. Since the interaction between the disc milling cutter and the workpiece is analytically expressed, the proposed approach is able to capture the chatter stability prediction for the face milling process of workpieces with discontinuous surfaces.

2.3 Chatter Stability Prediction. Since the stability lobe diagram method is effective and efficient to predict and avoid chatter in practical engineering, this section is devoted to obtain the SLD for the face milling process. The chatter stability is dependent on the dynamic response of the machining system, which is commonly expressed by FRF. For a 2-DOF cutter-workpiece vibration system, the FRF at the chatter frequency ω_c can be formulated as

$$[G(i\omega_c)] = \begin{bmatrix} G_{xx}(i\omega_c) & G_{xy}(i\omega_c) \\ G_{yx}(i\omega_c) & G_{yy}(i\omega_c) \end{bmatrix} \tag{20}$$

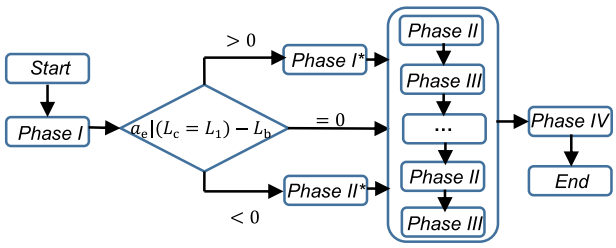

Fig. 7 Three passible cases for the face milling process

where i is the unit of imaginary number, and the chatter frequencies $\omega_c = \omega_{c1}, \omega_{c2}, \ldots, \omega_{cn}$ can be obtained by simulation or experiments, which are usually around the dominant modes of the vibration system.

Considering the regenerative effect, the dynamic cutting force model can be further derived as

$$\{F(t)\}e^{i\omega_c t} = \frac{1}{2}a_p K_t(1 - e^{-i\omega_c \tau})[A_0][G(i\omega_c)]\{F(t)\}e^{i\omega_c t} \tag{21}$$

where τ is the time delay, equivalent to the insert passing period, namely, $\tau = 60/\Omega N_c$.

The necessary and sufficient condition of nonsingular solutions to Eq. (21) is termed as the chatter characteristic equation, which is given by

$$\det\{[I] - \Lambda[G_0(i\omega_c)]\} = 0 \tag{22}$$

Therein, $[I]$ is the identity matrix, while $G_0(i\omega_c)$ is the directional coefficient transfer matrix defined by

$$G_0(i\omega_c) = \frac{2\pi}{N_c}[A_0]G(i\omega_c) \tag{23}$$

And Λ is the eigenvalue, which is given by

$$\Lambda = \frac{N_c}{4\pi}a_p K_t(1 - e^{-i\omega_c \tau}) \tag{24}$$

Note that Λ is a complex number. Denoting the imaginary part and the real part of Λ as Λ_I and Λ_R, respectively, Λ can be rewritten as $\Lambda = \Lambda_R + i\Lambda_I$. Substituting the Euler's formula [57] $e^{-i\omega_c \tau} = \cos(\omega_c \tau) - i\sin(\omega_c \tau)$ into Eq. (24) yields

$$\begin{cases} \Lambda_R = \frac{N_c}{4\pi}a_p K_t(1 - \cos(\omega_c \tau)) \\ \Lambda_I = \frac{N_c}{4\pi}a_p K_t \sin(\omega_c \tau) \end{cases} \tag{25}$$

And Eq. (25) can be further derived as

$$\frac{\Lambda_I}{\Lambda_R} = \frac{\sin(\omega_c \tau)}{1 - \cos(\omega_c \tau)} \tag{26}$$

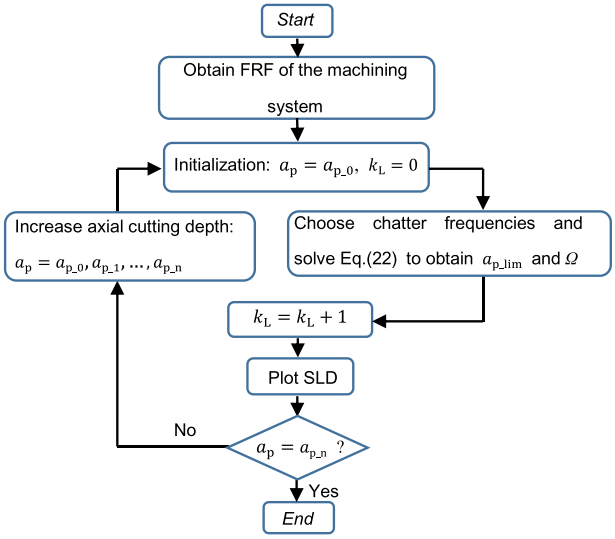

Fig. 8 Pseudo code for generating the stability lobe diagram for face milling process

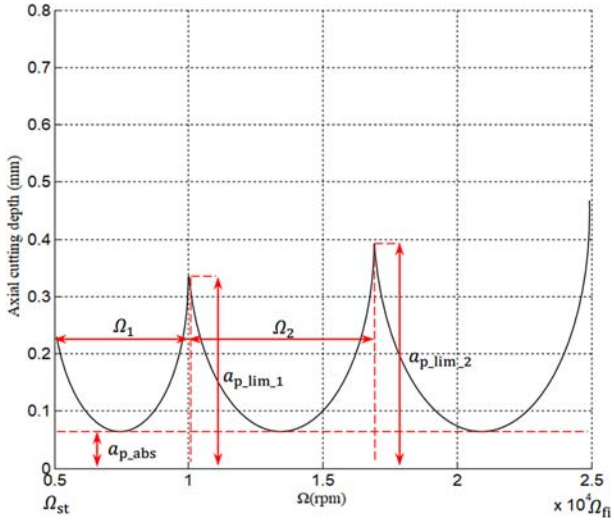

Fig. 9 Illustration of evaluation indexes used in sensitivity analysis

The critical value of the axial cutting depth can be calculated by

$$a_{p\_lim} = \frac{2\pi(\Lambda_R^2 + \Lambda_I^2)}{N_c K_t \Lambda_R} \tag{27}$$

And the corresponding spindle speed can be obtained by

$$\Omega = \frac{60}{N_c((2k_L + 1)\pi - 2\arctan(\Lambda_I/\Lambda_R))} \tag{28}$$

where $k_L = 0, 1, 2, \ldots$, which gives successive stability lobes.

The SLD can be generated by the following main steps, and the pseudo-code for programming is exhibited in Fig. 8.

Step 1: Establish the dynamic cutting force model considering cutting insert engagement and regenerative effect.
Step 2: Obtain the FRF $[G(i\omega_c)]$ at each chatter frequency based on the dynamic cutting force model.
Step 3: Select chatter frequencies $\omega_c = \omega_{c1}, \omega_{c2}, \ldots, \omega_{cn}$ around the dominate modes and scan each of them.
Step 4: Set the initial axial cutting depth $a_p = a_{p\_0}$.
Step 5: Calculate the critical axial cutting depth a_{p_lim} and the corresponding spindle speed Ω by solving the chatter characteristic equation (Eq. (22)).
Step 6: Increase the axial cutting depth gradually, namely, $a_p = a_{p\_0}, a_{p\_1}, \ldots, a_{p\_n}$, and repeat step 5.
Step 7: Assemble the critical axial cutting depth a_{p_lim} at each corresponding spindle speed Ω and then plot the chatter stability lobes.

Based on the SLD generated through the steps proposed above, the chatter stability can be predicted for face milling process of workpieces with discontinuous surfaces. The suitable process parameters should be chosen before the machining operation, so that chatter can be avoided as far as possible.

2.4 Sensitivity Analysis. The stability of face milling process are comprehensively affected by multiple process parameters including the feed per insert f_z, the axial cutting depth a_p, the spindle speed Ω, the total number of inserts N_c, and the diameter of the disc milling cutter D_c. Therefore, it is necessary to implement the sensitivity analysis for each relevant parameter before the optimization of process parameters. The axial cutting depth with respect to the absolute stability region, denoted by a_{p_abs}, is utilized to describe the critical characteristic of the SLD. As depicted in Fig. 9, a_{p_abs} is defined to evaluate the absolute "height" of the stability lobe curve.

Within the interval of spindle speed ranging from the starting speed Ω_{st} to the final speed Ω_{fi}, a qualitative analysis of the influence of different process parameters on the SLD can be obtained by using the single-variable method. According to engineering experience, the default set of parameters is given in Table 3.

Note that only the optimization of process parameters is concerned in this paper, thus all the geometric and material parameters of the workpiece are set to fixed levels. By changing the level of a single parameter from the default level and keeping the rest unchanged, a series of numerical experiments are conducted to generate the stability lobe curves and the results are shown as follows.

As depicted in Fig. 10, there is a downward trend in the stability lobes with the growth of f_z, leading to a nonlinear decline in a_{p_abs}.

Since the average cutting force is positively correlated with f_z according to Eq. (5), the forced vibrations caused by the dynamic interaction between the disc milling cutter and the workpiece will be aggravated when a larger f_z is chosen. Enlarging feed rate brings not only higher processing efficiency but also poorer processing stability, and this is one of the critical balances that should be considered in the optimization of process parameters.

Figure 11 exhibits the downward trend in the stability lobes with the growth of N_c. This trend is mainly caused by the increasing excitation frequency, which is in good agreement with the conclusions drawn by the classic publications [12,14]. However, since the processing efficiency is positively correlated with N_c, this is another critical balance that should be taken into consideration during optimizing process parameters.

The upward trend in the stability lobes with the growth of D_c is shown in Fig. 12. Based on Eqs. (14)–(19), it can be proved that the

Table 3 Default set of parameters given by engineering experience

Type	Parameter	Default level
Process	f_z (mm)	0.02
	D_c (mm)	160
	N_c	12
Geometric	R_b (mm)	35
	L_b (mm)	108
Material	E (GPa)	140
	υ	0.27

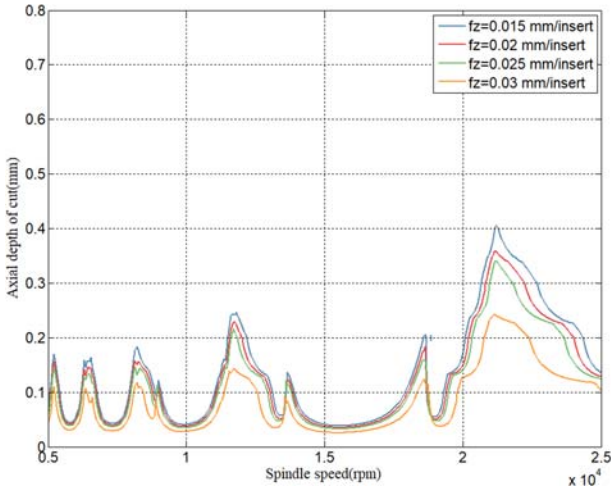

Fig. 10 Trend chart of stability lobe curves with varying feed per insert

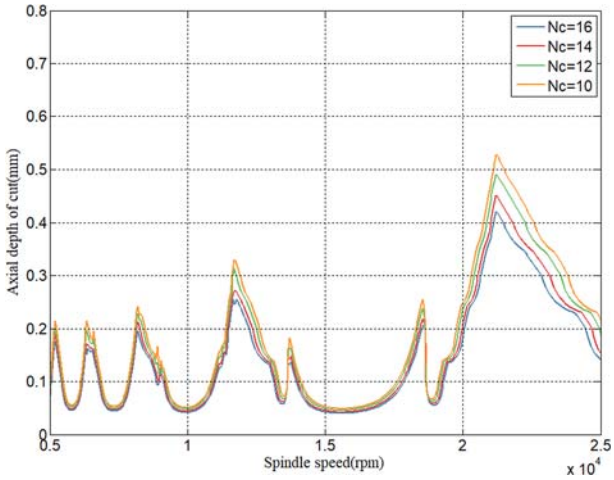

Fig. 11 Trend chart of stability lobe curves with varying number of inserts

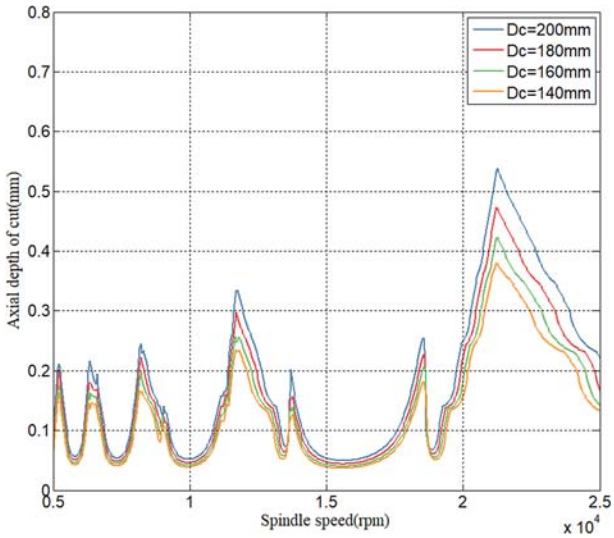

Fig. 12 Trend chart of stability lobe curves with varying diameter of disc milling cutter

number of inserts engaged with the workpiece N is a monotone decreasing function of the diameter of disc milling cutter D_c within a certain domain. Therefore, by appropriately enlarging D_c, the amplitude of forced vibration can be reduced and the dynamic stability of the machining system can be improved simultaneously. This verdict will be immensely helpful in simplifying the optimization model of process parameters in Sec. 2.5.

Based on the results of sensitivity analysis, an optimization model can be established and solved to improve processing efficiency with the consideration of processing stability and quality.

2.5 Optimization of Process Parameters. The ultimate goal of this paper is to improve the chatter-free processing efficiency. The material removal rate is one of the most commonly used indicators for processing efficiency, which is defined by

$$Q_{MRR} = a_p a_e f_z \Omega N_c \tag{29}$$

It can be seen that the higher the levels of process parameters are set, the larger the material removal rate will be. Note that all the factors on the right-hand side of Eq. (29), except the radial cutting depth a_e, are adjustable before machining, independent of each other and constant once set. However, due to the variable geometry of the workpiece, a_e varies with the cutting distance L_c during the whole face milling process. Thus, Q_{MRR} is time-varying and the mean value $\bar{Q}_{MRR}$ is needed for evaluating the processing efficiency, which is not convenient for the optimization modeling. To deal with this problem, a simplified objective function is proposed by this paper. According to Eq. (13), by regarding L_c as a constant, a_e becomes a monotone increasing function of D_c in *phase I*. And it can be proved that in the following phases of the face milling process, the mean value of a_e is independent of D_c due to the symmetry of cylindrical bores according to *hypothesis I*. In addition, according to the positive verdict on D_c given in Sec. 2.4, appropriately enlarging D_c is helpful in improving the dynamic stability of the system as well as raising the level of a_e. In other words, the objective of the optimization model can be simplified by setting D_c to the highest possible level D_c^*, removing a_e from the right-hand side of Eq. (29) and maximizing the product of the rest four factors, so that the processing efficiency is equivalently optimized. Therefore, the objective function is given as

$$\max \quad a_p f_z \Omega N_c \tag{30}$$

Main constraints in process parameter design are summarized as follows:

Constraint 1: The spindle speed Ω should be chosen within an appropriate range. The lower and upper bounds are jointly determined by material properties of the workpiece and the load capacity of the machine tool, which are set to Ω_{st} and Ω_{fi}, respectively, in this paper.

Constraint 2: In order to maintain the stability of the machining system and ensure that no chatter occurs during the face milling process, a_p should be less than the critical axial cutting depth $a_{p\_lim}(\Omega)$ corresponding to the spindle speed Ω. That is, the point with coordinates of (a_p, Ω) should be located in the stable region of the SLD.

Constraint 3: Since the evaluation indexes of the stability lobe curve worsen rapidly with the growth of f_z according to Sec. 2.4, there is no need to set an explicit upper bound for f_z while the lower bound is set to zero.

Constraint 4: Obviously, the total number of inserts N_c is a positive integer, and its highest possible level N_c^* is equal to the maximum number of inserts on a disc milling cutter with a diameter of D_c^*. Note that N_c is usually set to an even number to improve the symmetry of the cutting forces in engineering practice, which has significantly reduced the feasible domain of this problem.

Therefore, the optimization model is subjected to

$$\begin{cases} \Omega_{st} < \Omega < \Omega_{fi} \\ 0 < a_p < a_{p\_lim}(\Omega) \\ f_z > 0 \\ N_c \in \{2, 4, \ldots, N_c^*\} \end{cases} \tag{31}$$

Since the optimization model is nonlinear and complex according to Eqs. (30) and (31), the genetic algorithm (GA) is employed to solve the model. Based on the general procedures of GA, the key computation rules are listed as follows:

Rule for variable discretization: It is indicated by Eq. (31) that all the process parameters except N_c are continuous variables during the optimization process, which is not convenient for GA to solve the optimization model. Hence, a rule for variable discretization is necessary. The key point is to determine the search step size for each continuous variable. If the search step size is excessive, the GA will tend to be trapped by local optimal solutions and fail to find the global one. Conversely, if the search step size is too small, redundant computation will reduce the computing efficiency of the proposed approach. Besides, the process parameters with too much digits after the decimal place (i.e., exceeding the tuning accuracy of the machine tool) are meaningless for engineering practice. Therefore, taking solution effect, computing efficiency, and engineering applicability into consideration, the search step sizes for a_p, Ω, and f_z are set to 0.01 mm, 100 rpm, and 0.001 mm, respectively.

Rule for fitness computation: The fitness function is the only indicator for the suitability of a certain individual and the selection probability is calculated based on the rank of fitness values. As for GA, the fitness values should be always positive and the larger one is preferred, which is fortunately consistent with the objective function. Thus, the fitness value of a certain individual is equal to the product of a_p, f_z, Ω, and N_c in this paper.

Rule for selection, crossover, and mutation: In order to increase the robustness of the optimization process, a roulette-wheel selection algorithm [58] is implemented. Two chromosomes are randomly selected based on the cumulative distribution function of fitness, instead of simply selected by maximum fitness, as the objects for crossover and mutation. The crossover probability is set to a constant, whereas the mutation probability is a piecewise increasing function of generations, so as to improve the ability to escape from the local optimal solutions.

Rule for stopping criteria: The iteration of the optimization process will be stopped if and only if the maximum fitness is continuously maintained at a certain level for a given number of generations, which is set to 200 in this paper, and then the GA is deemed to converge to the global optimal solution.

3 Case Study

3.1 Dynamic Cutting Force Measurement. In order to validate the proposed dynamic cutting force model considering the effect of cutting insert engagement, six sets of face milling experiments with different process parameters are carried out for dynamic cutting force measurement. The detailed process parameters for cutting force measurement are given in Table 4.

The experimental setup for dynamic cutting force measurement is illustrated in Fig. 13. The machining operations are conducted in a CNC machining center of type DMG-HSC-75 (see Fig. 13(*a*)). According to the type of the CNC, the highest possible level of the diameter of the disc milling cutter is 200 mm. Thus, D_c^* is set to 200 mm in this paper. Cutting fluid of type Quaker-370-KLG is used during the face milling process. The components of the dynamic cutting force are measured by three-component dynamometer of type Kistler-9027C (see Fig. 13(*b*)). The acceleration sensors of the dynamometer are embedded in the vise to detect the signals of dynamic cutting forces. The sampling period for each single operation is set to 30 s. The whole experimental process is under closely supervised conditions to ensure that no anomalous problems emerge.

The frequency response functions of the machine tool system can be identified by impact testing. The cantilever length of the disc milling cutter is 70 mm. In order to reduce the impact uncertainty, the impact testing is conducted three times in each direction, and the mean value of the obtained FRFs is taken as the measurement results. The "Peak-picking" method [59] is utilized to identify the modal parameters of the machine tool system. The real parts and imaginary parts of the measured FRFs are presented by Fig. 14. Note that the cross FRFs of the machine tool system are deemed as identical in this paper.

Limited by the size of the dynamometer vise (with maximum opening distance about 100 mm), the face milling operations are performed on the top surface of a quarter of the four-cylinder

Table 4 Experiment design for cutting force measurement

Case No.	f_z (mm)	a_p (mm)	Ω (rpm)	N_c
(1-1)	0.01	0.05	5000	6
(1-2)	0.02	0.2	28,000	8
(1-3)	0.016	0.13	15,000	10
(1-4)	0.012	0.28	20,000	8
(1-5)	0.024	0.15	17,000	10
(1-6)	0.026	0.22	23,000	6

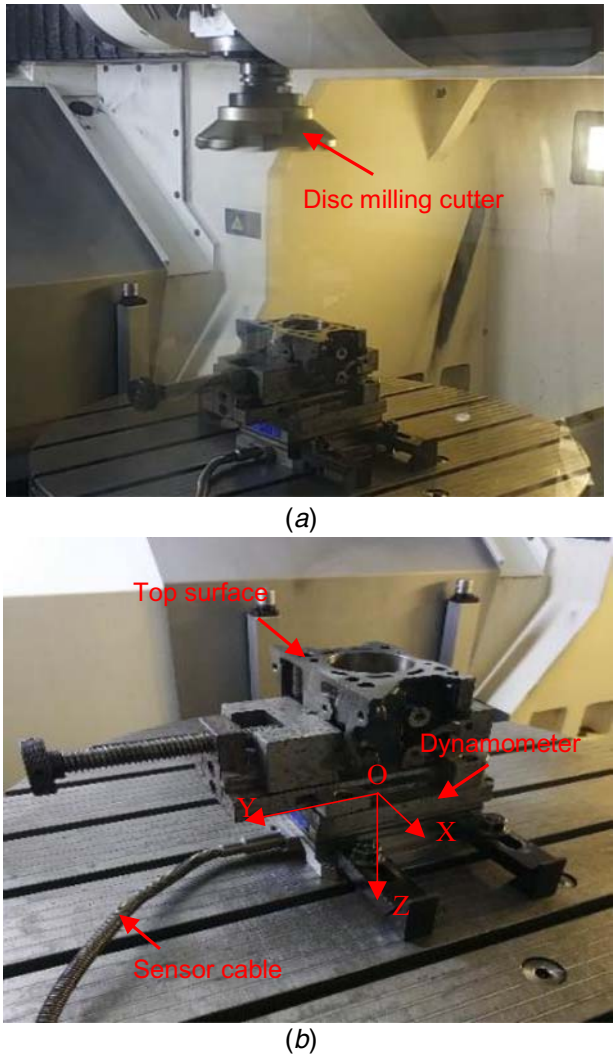

Fig. 13 Experimental setup for dynamic cutting force measurement: (*a*) CNC machining center and (*b*) fixturing by the dynamometer vise

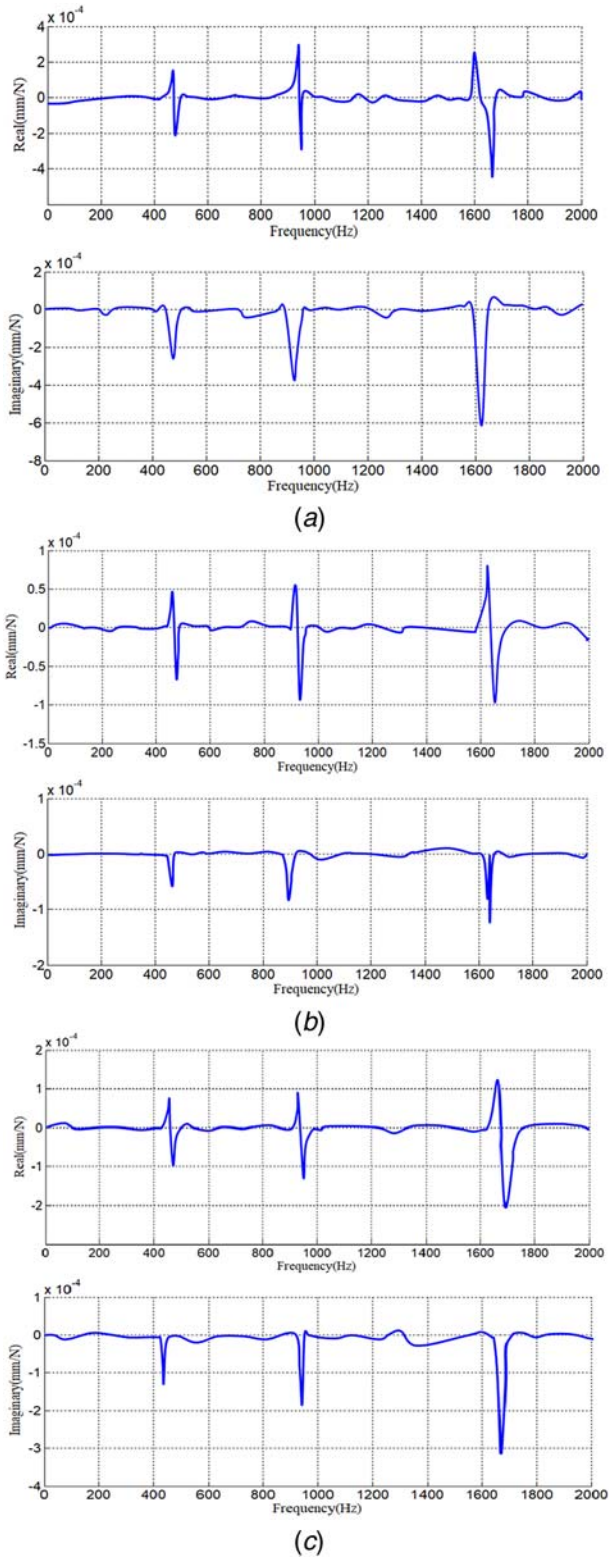

Fig. 14 Frequency response functions of the machine tool system: (*a*) G_{xx}, (*b*) G_{xy}, and (c) G_{yy}

engine block made of gray cast iron (HT250). Since a complete cylinder bore is contained in this quarter, the most representative geometric characteristics of the engine block are reserved. And the analysis of cutting insert engagement proposed in Sec. 2.2 is still applicable for this case. Based on the geometry dimensions of the disc milling cutter and the engine block given in Table 5, it can be obtained that $\sqrt{D_c^2 - (D_c - 2L_1)^2}$ is around 111.6 mm, which is larger than L_b. Therefore, the cutting insert engagement, in this case, can be calculated with the emergence of *phase I**.

During the experimental process, it is found that chatter occurs in case (1-2) whereas other cases are relatively stable. Taking case (1-4) as an example of stable cutting contrast to case (1-2), the dynamic cutting force components along *X*-axis and the corresponding spectra are shown in Fig. 15. Both in the stable cutting case and the chatter case, there are two peaks and one trough in the cutting force waveform (see Figs. 15(*a*) and 15(*c*)). In other words, the magnitude of cutting force increases first and then decreases and increases again as the face milling proceeds. When the disc milling cutter reaches the nearest generatrix of the cylinder bore, the length of cutting arc starts to decrease, and the number of inserts engaged with the workpiece declines as well. However, when the center of the cylinder bore is passed through by the edge of the disc milling cutter, both of them rise again. The magnitude of cutting force shares the same trend with the cutting insert engagement. Moreover, for the stable cutting case (1-4), the dominant frequency of the cutting forces is equivalent to the tool passing frequency 330 Hz (see Fig. 15(*b*)). Due to chatter vibrations, however, the magnitude of cutting force in chatter case (1-2) increases significantly and the chatter frequency 1650 Hz becomes dominant (see Fig. 15(*d*)), which is approximately equal to one of the natural frequencies of the machining system. Therefore, the experiment results are reasonable and consistent with the proposed theories.

3.2 Validation of Optimized Process Parameters. To validate the advantages of the proposed approach, a classic approach [29] is utilized to generate the default design of process parameters for comparison. By solving the optimization model aimed at maximizing the equivalent processing efficiency with GA, the optimal design of process parameters is obtained, and the comparison between the default design and optimized design of process parameters is given in Table 6.

The fitness convergence of GA is shown by Fig. 16. It is found that there is a staged increase in maximum fitness as generation grows from 1 to 1000. The stopping criteria are eventually satisfied due to the maximum fitness has been continuously maintained at 3380.3 for over 200 generations, which means that the iteration process has converged to the global optimal solution. Note that the default design of process parameters is directly leaped over during the optimization process, illustrated by the red dashed line in Fig. 16, which is a normal phenomenon for GA [60,61].

The SLDs with the optimized and default sets of process parameters are plotted by MATLAB R2013B programming, respectively, as shown in Fig. 17. It is found that the optimized SLD has been evidently improved on the default one. To validate the chatter prediction accuracy of the SLDs generated by the proposed approach, 30 sets of face milling experiments are conducted on the top surface of a complete four-cylinder engine block. For the optimized SLD, 10 cubic boron nitride (CBN) inserts and a disc milling cutter with a diameter of 200 mm are used, and the feed per insert f_z is set to

Table 5 Geometry dimensions (mm) for cutting insert engagement

D_c	L_1	L_2	L_3	L_4	L_5	L_6	L_7	L_8	L_a	L_b	R_b
200	17	87	92.5	162.5	168	238	243.5	313.5	326	108	35

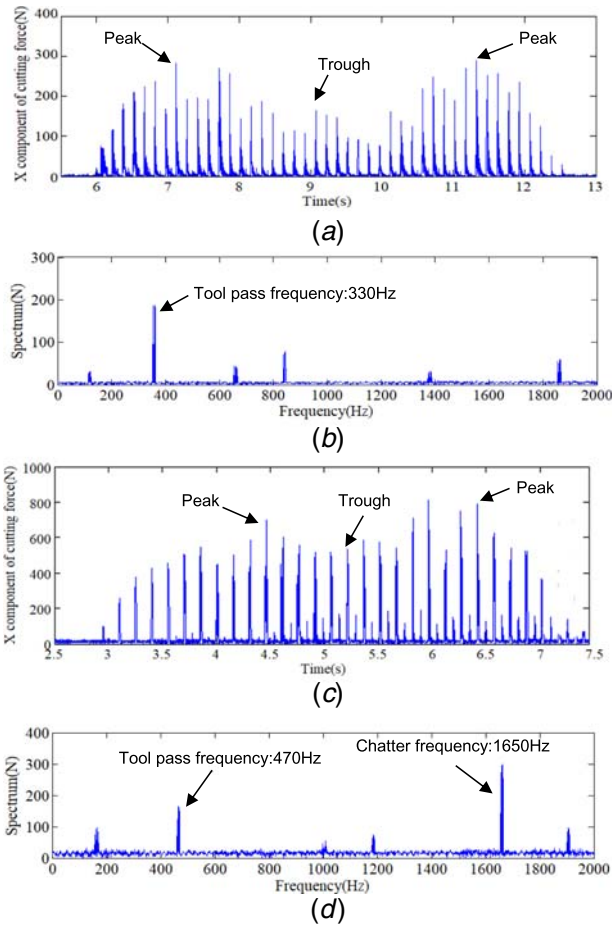

Fig. 15 Dynamic cutting forces and spectra for stable cutting case and chatter case: (*a*) dynamic cutting forces of stable cutting case (1-4), (*b*) cutting force spectrum of stable cutting case (1-4), (*c*) dynamic cutting forces of chatter case (1-2), and (*d*) cutting force spectrum of chatter case (1-2)

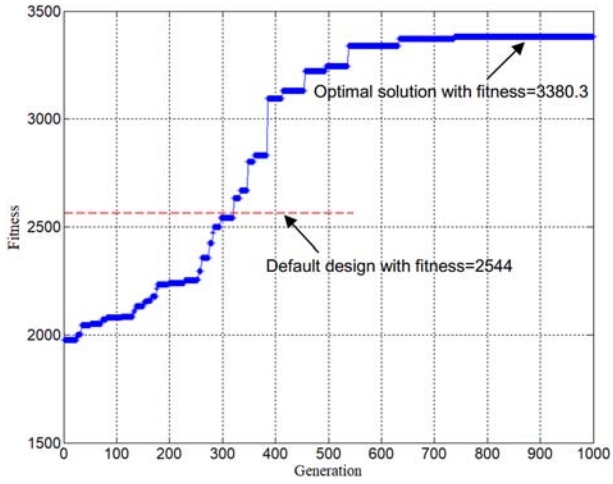

Fig. 16 The trend of the maximum fitness value as generation grows

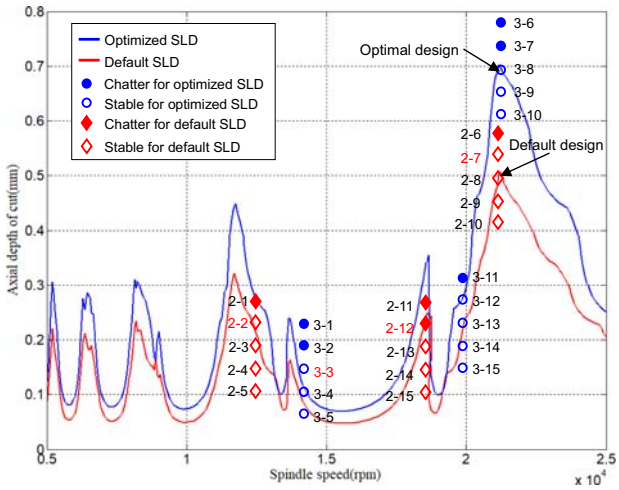

Fig. 17 Predicted and measured chatter stability results

0.023 mm. For the default SLD, 12 CBN inserts and a disc milling cutter with a diameter of 160 mm are used, and f_z is set to 0.02 mm. The detailed information about the axial cutting depth a_p and spindle speed Ω is given in Table 7.

All of these 30 experimental cases are marked as red diamonds and blue circles in Fig. 17. For the default SLD, ten experimental cases are numbered from (2-1) to (2-15), where the hollow diamonds refer to stable cutting cases and the solid ones refer to chatter cases. For the optimized SLD, the rest ten experimental cases are numbered from (3-1) to (3-15), where the hollow circles refer to stable cutting cases and the solid ones refer to chatter cases. Of note is that case (2-8) and case (3-8) are conducted with the default design and the optimal design of process parameters, respectively. And both of them present stable cutting process, which is consistent with the SLDs given by the proposed approach.

Table 6 Comparison between the default design and optimized design

Process parameter	Default design	Optimized design
f_z (mm)	0.02	0.023
D_c (mm)	160	200
N_c	12	10
a_p (mm)	0.5	0.69
Ω (rpm)	21,200	21,300

It is found that case (3-3) should be unstable according to the optimized SLD; however, no chatter occurs during the machining process of case (3-3) indeed. Regardless of the experimental errors, there are two possible reasons for this false alarm. On the one hand, the axial cutting depth and the spindle speed

Table 7 Axial cutting depth and spindle speed for validation of chatter prediction

Default SLD			Optimized SLD		
Case no.	a_p (mm)	Ω (rpm)	Case No.	a_p (mm)	Ω (rpm)
(2-1)	0.27	12,500	(3-1)	0.23	14,200
(2-2)	0.23	12,500	(3-2)	0.19	14,200
(2-3)	0.19	12,500	(3-3)	0.15	14,200
(2-4)	0.15	12,500	(3-4)	0.11	14,200
(2-5)	0.11	12,500	(3-5)	0.07	14,200
(2-6)	0.58	21,200	(3-6)	0.77	21,300
(2-7)	0.54	21,200	(3-7)	0.73	21,300
(2-8)	0.5	21,200	(3-8)	0.69	21,300
(2-9)	0.46	21,200	(3-9)	0.65	21,300
(2-10)	0.42	21,200	(3-10)	0.61	21,300
(2-11)	0.27	18,300	(3-11)	0.31	19,900
(2-12)	0.23	18,300	(3-12)	0.27	19,900
(2-13)	0.19	18,300	(3-13)	0.23	19,900
(2-14)	0.15	18,300	(3-14)	0.19	19,900
(2-15)	0.11	18,300	(3-15)	0.15	19,900

used in case (3-3) are adjacent to one of the sub-lobes of the optimized SLD, which might be induced by the computational deviation of geometric characteristics of the engine block. That is, the simplification of the engine block brings not only convenience but also deviation to computation, leading to sub-lobes nearby the critical axial cutting depth. On the other hand, chatter prediction is a complex problem involving multiple factors such as dynamic behavior of the machine spindle and the stability of the fixture system, which are considered to be controlled variables and kept fixed in this paper. These factors might affect the prediction accuracy to a certain degree. Nevertheless, the chatter prediction based on the proposed approach is sufficiently effective with an acceptable accuracy, which demonstrates that the optimization of process parameters is based on a valid dynamic model.

The experimental setup is shown in Fig. 18. The 3-2-1 locating principle is implemented for the fixturing scheme, and the engine block is located and clamped by a self-designed fixture (see Fig. 18(*a*)). And the flatness of the machined surface is measured by the coordinate measurement machine (CMM) system of type LEITZ-PMM-XI (see Fig. 18(*b*)). For each measurement, 50 points randomly distributed on the top surface are selected and measured by the CMM probe. Taking case (2-3), case (3-2), case (2-8), and case (3-8) as instances, the measurement results are shown in Fig. 19.

Obviously, the surface quality of the stable cutting case (case (2-3), case (2-8), and case (3-8)) is much better than that of the chatter case (case (3-2)). The flatness of the machined surface for

(*a*)

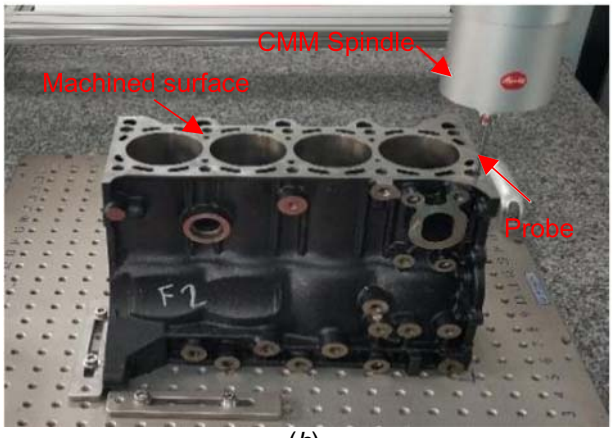

(*b*)

Fig. 18 Experimental setup for validation of optimized process parameters: (*a*) face milling process on the four-cylinder engine block and (*b*) flatness measurement by the CMM system

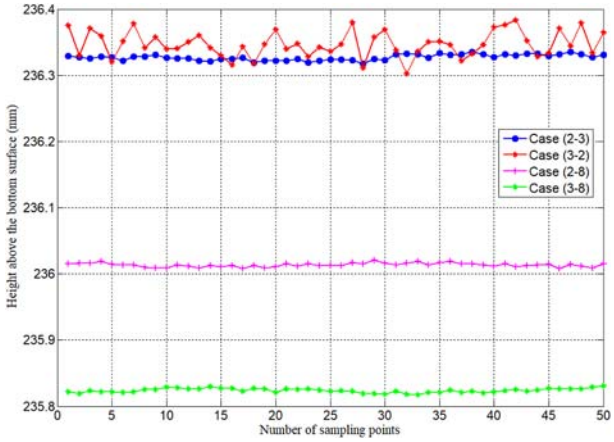

Fig. 19 Measured heights of the sampling points

each case can be obtained by using the least square method. And the average MRR of each case can be calculated by Eqs. (13) and (29). The computation results are given in Table 8.

It is found that chatter not only increases the flatness but also leads to bias of mean height of the machined surface (around 0.02 mm higher than expected), which has further demonstrated the significance of chatter prediction to finish surface quality. The calculation results also indicate that the proposed approach has improved the average MRR by nearly 53.3% (from 178589 mm^3/min to 273805 mm^3/min). In addition, as the average MRR is improved significantly by optimizing process parameters in the condition of chatter-free, the machined surface quality is ensured as well.

4 Conclusion

In this paper, an analytical approach for process parameter optimization is proposed based on dynamics modeling of the face milling process of workpieces with discontinuous surfaces. A novel dynamic cutting force model is constructed, comprehensively considering the effects of cutting insert engagement. This research provides an effective way to optimize the process parameters to improve the chatter-free processing efficiency, taking a four-cylinder engine block as an instance.

The face milling process is divided into several phases, and the dynamic behaviors for each phase are calculated based on the cutting insert engagement. In addition, SLDs with acceptable accuracy are built for chatter prediction for the face milling process of a typical workpiece with discontinuous surfaces. To quantify the effect of different process parameters on the SLD, the sensitivity analysis is given. Based on the verdicts of the sensitivity analysis, an optimization model aimed at maximizing the equivalent MRR is constructed, and the GA is employed to solve the optimization model. To demonstrate the effectiveness of the proposed approach, a series of machining experiments are conducted for dynamic cutting force measurement and validation of optimization process parameters. The experimental results are in good agreement with the theoretical results, indicating that the proposed approach can effectively improve the processing efficiency without loss of machined surface quality.

Since the top surface of a four-cylinder engine block is a typical discontinuous surface, it makes sense to deal with workpieces with other types of discontinuous surfaces in the optimization of process parameters by the proposed approach for its successful application to the engine block. The proposed approach can provide a guideline for industrial engineers to maximize the chatter-free processing efficiency by selecting the optimal levels of relevant process parameters during the design stage.

For future work, more internal factors that affect the chatter stability such as a gyroscopic moment of spindle and fixture stiffness

Table 8 Experimental results for each case

Case no.	(2-3)	(3-2)	(2-8)	(3-8)
Mean height of machined surface (mm)	236.33	236.35	236.02	235.83
Flatness of machined surface (mm)	0.0226	0.0721	0.0230	0.0232
Average MRR (mm^3/min)	67,864	75,396	178,589	273,805

should be taken into consideration. Furthermore, it will be concerned that how to determine the interaction between the cutter and workpiece for peripheral milling or end milling, so as to improve the generality of the proposed dynamic model.

Acknowledgment

This research was supported by the National Natural Science Foundation of China (Grant Nos. 51535007 and 51775343; Funder ID: 10.13039/501100001809). The authors are grateful to Shanghai Automotive Industry Corporation General Motors Wuling Company in Liuzhou, China, for providing engine blocks for experiments.

Nomenclature

E = elastic modulus (MPa)
M = number of microelements of each insert
N = number of inserts engaged with the workpiece
a_e = radial cutting depth (mm)
a_p = axial cutting depth (mm)
a_{p_abs} = axial cutting depth w.r.t. the absolute stability region (mm)
k_L = serial number of stability lobes
t_c = cutting duration (s)
D_c = diameter of the disc milling cutter (mm)
L_a = length of the engine block (mm)
L_b = width of the engine block (mm)
L_c = cutting distance (mm)
N_c = total number of inserts
R_b = radius of the cylindrical bore (mm)
R_c = ideal cutter radius (mm)
V_c = cutting speed (mm/s)
V_f = feed rate (mm/s)
$\bar{Q}_{MRR}$ = mean value of material removal rate (mm^3/min)
f_z = feed per insert (mm)
Q_{MRR} = material removal rate (mm^3/min)
D_c^* = highest possible level of D_c (mm)
N_c^* = maximum number of inserts on a disc milling cutter with a diameter of D_c^*
$a_{p\_lim}(\Omega)$ = critical axial cutting depth function of Ω (mm)
c_x; c_y = damping of the cutter-workpiece system along X-axis and Y-axis
m_x; m_y = mass of the cutter-workpiece system along X-axis and Y-axis
k_x; k_y = stiffness of the cutter-workpiece system along X-axis and Y-axis
$A(t)$ = directional coefficient matrix
$[A_0]$ = time-invariant directional coefficient matrix
A_x; A_y; A_z = corresponding undetermined coefficients
B_x; B_y; B_z = substituting undetermined coefficients
$F_{A,x}$; $F_{A,y}$; $F_{A,z}$ = average cutting forces along X, Y, and Z axes (N)
F_x; F_y; F_z = cutting forces along X, Y, and Z axes (N)
$[G(i\omega_c)]$ = frequency response function at chatter frequency ω_c
$G_0(i\omega_c)$ = directional coefficient transfer matrix
K_r; K_t; K_a = radial, tangential and axial cutting parameter coefficients
L_1; L_2; … L_7 = geometry parameters of the engine block (mm)
β = angle of the flank edge (deg)
ΔL_c = microelement of cutting distance (mm)
$\{\Delta(t)\}$ = regeneration displacement vector at the moment t
$\theta_{1,0}$ = angular displacement of the bottom of the first tooth (deg)
$\theta_{j,l}$ = radial immersion angle of the ith microelement of the jth tooth ($j = 1, 2, \ldots N$; $l = 1, 2, \ldots, M$) (deg)
θ_{st}; θ_{ex} = starting cut angle; exiting cut angle (deg)
Λ_I = imaginary part of the eigenvalue
Λ_R = real part of the eigenvalue
υ = Poisson ratio
ω_c = chatter frequency (Hz)
Ω = spindle speed (rpm)
Ω_{fi} = final spindle speed for SLD
Ω_{st} = starting spindle speed for SLD

Appendix

The distance between the centers of the disc milling cutter and the first cylindrical bore can be formulated as

$$L_{y1} = \frac{D_c}{2} + R_b - L_c + L_1 \tag{A1}$$

According to the Heron's Formula, the area of the triangular $Q_1O_cO_b$ can be given by

$$S_{t1} = \sqrt{p\left(p - \frac{D_c}{2}\right)(p - R_b)(p - L_{y1})} \tag{A2}$$

where p is an intermediate parameter given by

$$p = \frac{1}{2}\left(\frac{D_c}{2} + R_b + L_{y1}\right) \tag{A3}$$

References

[1] Wang, M., Ken, T., Du, S., and Xi, L., 2015, "Tool Wear Monitoring of Wiper Inserts in Multi-Insert Face Milling Using Three-Dimensional Surface Form Indicators," ASME J. Manuf. Sci. Eng., **137**(3), p. 031006.
[2] Du, S., Liu, C., and Huang, D., 2015, "A Shearlet-Based Separation Method of 3D Engineering Surface Using High Definition Metrology," Precis. Eng., **40**, pp. 55–73.
[3] Shao, Y., Yin, Y., Du, S., Xia, T., and Xi, L., 2018, "Leakage Monitoring in Static Sealing Interface Based on Three Dimensional Surface Topography Indicator," ASME J. Manuf. Sci. Eng., **140**(10), p. 101003.
[4] Abele, E., and Fiedler, U., 2004, "Creating Stability Lobe Diagrams During Milling," CIRP Ann., **53**(1), pp. 309–312.
[5] Du, S., Liu, C., and Xi, L., 2015, "A Selective Multiclass Support Vector Machine Ensemble Classifier for Engineering Surface Classification Using High Definition Metrology," ASME J. Manuf. Sci. Eng., **137**(1), p. 011003.
[6] Eksioglu, C., Kilic, Z. M., and Altintas, Y., 2012, "Discrete-time Prediction of Chatter Stability, Cutting Forces, and Surface Location Errors in Flexible Milling Systems," ASME J. Manuf. Sci. Eng., **134**(6), p. 061006.
[7] Du, S., Huang, D., and Wang, H., 2015, "An Adaptive Support Vector Machine-Based Workpiece Surface Classification System Using High Definition Metrology," IEEE Trans. Instrum. Meas., **64**(10), pp. 2590–2604.
[8] Suriano, S., Wang, H., Shao, C., Hu, S. J., and Sekhar, P., 2015, "Progressive Measurement and Monitoring for Multi-Resolution Data in Surface Manufacturing Considering Spatial and Cross Correlations," IIE Trans., **47**(10), pp. 1033–1052.
[9] Suriano, S., Wang, H., and Hu, S. J., 2012, "Sequential Monitoring of Surface Spatial Variation in Automotive Machining Processes Based on High Definition Metrology," J. Manuf. Syst., **31**(1), pp. 8–14.
[10] Tobias, S. A., 1965, *Machine Tool Vibration*, Wiley, New York.

[11] Tlusty, J., 1999, *Manufacturing Process and Equipment*, Prentice Hall, New Jersey.
[12] Sridhar, R., Hohn, R. E., and Long, G. W., 1968, "A Stability Algorithm for the General Milling Process," ASME J. Eng. Ind., **90**(2), pp. 330–334.
[13] Zheng, C. M., Wang, J. J. J., and Sung, C. F., 2014, "Analytical Prediction of the Critical Depth of Cut and Worst Spindle Speeds for Chatter in End Milling," ASME J. Manuf. Sci. Eng., **136**(1), p. 011003.
[14] Minis, I., Yanushevsky, R., Tembo, A., and Hocken, R., 1990, "Analysis of Linear and Nonlinear Chatter in Milling," CIRP Ann., **39**(1), pp. 459–462.
[15] Minis, I., and Yanushevsky, R., 1993, "A New Theoretical Approach for the Prediction of Machine Tool Chatter in Milling," J. Eng. Ind., **115**(1), pp. 1–8.
[16] Movahhedy, M. R., and Mosaddegh, P., 2006, "Prediction of Chatter in High Speed Milling Including Gyroscopic Effects," Int. J. Mach. Tool Manuf., **46**(9), pp. 996–1001.
[17] Ding, Y., Zhu, L., Zhang, X., and Ding, H., 2010, "A Full-Discretization Method for Prediction of Milling Stability," Int. J. Mach. Tool Manuf., **50**(5), pp. 502–509.
[18] Li, Z., Yang, Z., Peng, Y., Zhu, F., and Ming, X., 2016, "Prediction of Chatter Stability for Milling Process Using Runge-Kutta-Based Complete Discretization Method," Int. J. Adv. Manuf. Technol., **86**(1–4), pp. 943–952.
[19] Dai, Y., Li, H., Xing, X., and Hao, B., 2018, "Prediction of Chatter Stability for Milling Process Using Precise Integration Method," Precis. Eng., **52**, pp. 152–157.
[20] Ismail, F., and Soliman, E., 1997, "A New Method for the Identification of Stability Lobes in Machining," Int. J. Mach. Tools Manuf., **37**(6), pp. 763–774.
[21] Lee, S., and Park, J. K., 2018, "Experimental Verification of Dynamic Behavior of a Capsule-Type Modular Machine Tool for Multifunctional Processes," ASME J. Manuf. Sci. Eng., **140**(1), p. 014501.
[22] Tuysuz, O., and Altintas, Y., 2018, "Time-Domain Modeling of Varying Dynamic Characteristics in Thin-Wall Machining Using Perturbation and Reduced-Order Substructuring Methods," ASME J. Manuf. Sci. Eng., **140**(1), p. 011015.
[23] Tuysuz, O., and Altintas, Y., 2017, "Frequency Domain Prediction of Varying Thin-Walled Workpiece Dynamics in Machining," ASME J. Manuf. Sci. Eng., **139**(7), p. 071013.
[24] Smith, S., and Tlusty, J., 1993, "Efficient Simulation Programs for Chatter in Milling," CIRP Ann., **42**(1), pp. 463–466.
[25] Cao, H., Li, B., and He, Z., 2012, "Chatter Stability of Milling with Speed-Varying Dynamics of Spindles," Int. J. Mach. Tool Manuf., **52**(1), pp. 50–58.
[26] Quintana, G., Ciurana, J., Ferrer, I., and Rodriguez, C. A., 2009, "Sound Mapping for Identification of Stability Lobe Diagrams in Milling Processes," Int. J. Mach. Tools Manuf., **49**(3), pp. 203–211.
[27] Altintas, Y., and Budak, E., 1995, "Analytical Prediction of Stability Lobes in Milling," CIRP Ann. Manuf. Technol., **44**(1), pp. 357–362.
[28] Merdol, S. D., and Altintaş, Y., 2014, "Multi Frequency Solution of Chatter Stability for Low Immersion Milling," ASME J. Manuf. Sci. Eng., **126**(3), pp. 459–466.
[29] Jensen, S. A., and Shin, Y. C., 1999, "Stability Analysis in Face Milling Operations, Part 1: Theory of Stability Lobe Prediction," ASME J. Manuf. Sci. Eng., **121**(4), pp. 600–605.
[30] Jensen, S. A., and Shin, Y. C., 1999, "Stability Analysis in Face Milling Operations, Part 2: Experimental Validation and Influencing Factors," ASME J. Manuf. Sci. Eng., **121**(4), pp. 606–614.
[31] Niu, J., Ding, Y., Geng, Z., Zhu, L., and Ding, H., 2018, "Patterns of Regenerative Milling Chatter Under Joint Influences of Cutting Parameters, Tool Geometries, and Runout," ASME J. Manuf. Sci. Eng., **140**(12), p. 121004.
[32] Caliskan, H., Kilic, Z. M., and Altintas, Y., 2018, "On-Line Energy-Based Milling Chatter Detection," ASME J. Manuf. Sci. Eng., **140**(11), p. 111012.
[33] Tang, X., Zhu, Z., Yan, R., Chen, C., Peng, F., Zhang, M., and Li, Y., 2018, "Stability Prediction Based Effect Analysis of Tool Orientation on Machining Efficiency for Five-Axis Bull-Nose End Milling," ASME J. Manuf. Sci. Eng., **140**(12), p. 121015.
[34] Baek, D. K., Ko, T. J., and Kim, H. S., 2001, "Optimization of Feedrate in a Face Milling Operation Using a Surface Roughness Model," Int. J. Mach. Tools Manuf., **41**(3), pp. 451–462.
[35] Song, Q., Ju, G., Liu, Z., and Ai, X., 2014, "Subdivision of Chatter-Free Regions and Optimal Cutting Parameters Based on Vibration Frequencies for Peripheral Milling Process," Int. J. Mech. Sci., **83**, pp. 172–183.
[36] Zhang, X., and Ding, H., 2013, "Note on a Novel Method for Machining Parameters Optimization in a Chatter-Free Milling Process," Int. J. Mach. Tools Manuf., **72**, pp. 11–15.
[37] Zhang, X., Zhu, L., Zhang, D., Ding, H., and Xiong, Y., 2012, "Numerical Robust Optimization of Spindle Speed for Milling Process with Uncertainties," Int. J. Mach. Tools Manuf., **61**, pp. 9–19.
[38] Zhang, X., Zhang, D., Cao, L., Huang, T., Leopold, J., and Ding, H., 2017, "Minimax Optimization Strategy for Process Parameters Planning: Toward Interference-Free Between Tool and Flexible Workpiece in Milling Process," ASME J. Manuf. Sci. Eng., **139**(5), p. 051010.
[39] Nguyen, H., Wang, H., and Hu, S., 2012, "Characterization of Cutting Force Induced Surface Shape Variation Using High-Definition Metrology," ASME 2012 International Manufacturing Science and Engineering Conference, Notre Dame, IN, June 4–8, pp. 641–650.
[40] Wang, M., Shao, Y., Du, S., and Xi, L., 2015, "A Diffusion Filter for Discontinuous Surface Measured by High Definition Metrology," Int. J. Precis. Eng. Manuf., **16**(10), pp. 2057–2062.
[41] Altintas, Y., and Lee, P., 1996, "A General Mechanics and Dynamics Model for Helical End Mills," ClRP Ann., **45**(1), pp. 59–64.
[42] Huang, D., Du, S., Li, G., and Wu, Z., 2017, "A Systematic Approach for Online Minimizing Volume Difference of Multiple Chambers in Machining Processes Based on High-Definition Metrology," ASME J. Manuf. Sci. Eng., **139**(8), p. 081003.
[43] Huang, D., Du, S., Li, G., Zhao, C., and Deng, Y., 2018, "Detection and Monitoring of Defects on Three-Dimensional Curved Surfaces Based on High-Density Point Cloud Data," Precis. Eng., **53**, pp. 79–95.
[44] Li, G., Du, S., Huang, D., Zhao, C., and Deng, Y., 2019, "Elastic Mechanics-Based Fixturing Scheme Optimization of Variable Stiffness Structure Workpieces for Surface Quality Improvement," Precis. Eng., **56**, pp. 343–363.
[45] Du, S., Liu, T., Huang, D., and Li, G., 2018, "A Fast and Adaptive Bi-Dimensional Empirical Mode Decomposition Approach for Filtering of Workpiece Surfaces Using High Definition Metrology," J. Manuf. Syst., **46**, pp. 247–263.
[46] Zhang, J. Z., Chen, J. C., and Kirby, E. D., 2007, "Surface Roughness Optimization in an End-Milling Operation Using the Taguchi Design Method," J. Mater. Process. Technol., **184**(1–3), pp. 233–239.
[47] Asiltürk, I., and Neşeli, S., 2012, "Multi Response Optimisation of CNC Turning Parameters via Taguchi Method-Based Response Surface Analysis," Measurement, **45**(4), pp. 785–794.
[48] Mhapsekar, K., McConaha, M., and Anand, S., 2018, "Additive Manufacturing Constraints in Topology Optimization for Improved Manufacturability," ASME J. Manuf. Sci. Eng., **140**(5), p. 051017.
[49] Lu, H. S., Chang, C. K., Hwang, N. C., and Chung, C. T., 2009, "Grey Relational Analysis Coupled With Principal Component Analysis for Optimization Design of the Cutting Parameters in High-Speed End Milling," J. Mater. Process. Technol., **209**(8), pp. 3808–3817.
[50] Pang, L., and Kishawy, H. A., 2012, "Modified Primary Shear Zone Analysis for Identification of Material Mechanical Behavior During Machining Process Using Genetic Algorithm," ASME J. Manuf. Sci. Eng., **134**(4), p. 041003.
[51] Kim, H. S., and Ehmann, K. F., 1993, "A Cutting Force Model for Face Milling Operations," Int. J. Mach. Tools Manuf., **33**(5), pp. 651–673.
[52] Wan, M., Zhang, W., Dang, J., and Yang, Y., 2009, "New Procedures for Calibration of Instantaneous Cutting Force Coefficients and Cutter Runout Parameters in Peripheral Milling," Int. J. Mach. Tools Manuf., **49**(14), pp. 1144–1151.
[53] Wan, M., Pan, W., Zhang, W., Ma, Y., and Yang, Y., 2014, "A Unified Instantaneous Cutting Force Model for Flat End Mills with Variable Geometries," J. Mater. Process. Technol., **214**(3), pp. 641–650.
[54] Budak, E., and Altintas, Y., 1998, "Analytical Prediction of Chatter Stability in Milling-Part I: General Formulation," J. Dyn. Syst., Meas., Control, **120**(1), pp. 22–30.
[55] Budak, E., and Altintas, Y., 1998, "Analytical Prediction of Chatter Stability in Milling-Part II: Application of the General Formulation to Common Milling Systems," J. Dyn. Syst., Meas., Control, **120**(1), pp. 31–36.
[56] Dunham, W., 1990, *Journey Through Genius: The Great Theorems of Mathematics*, Wiley, New York.
[57] Svetlik, M., Radojicic, M., Radovic, S., and Simic-Muller, K., 2018, "Justifying Euler's Formula Through Motion in a Plane," Math. Enthusiast, **15**(3), pp. 397–406.
[58] Aderiani, A. R., Wärmefjord, K., and Söderberg, R., 2018, "A Multistage Approach to the Selective Assembly of Components Without Dimensional Distribution Assumptions," ASME J. Manuf. Sci. Eng., **140**(7), p. 071015.
[59] Schmitz, T. L., and Smith, K. S., 2008, *Machining Dynamics: Frequency Response to Improved Productivity*, Springer Science & Business Media, Berlin.
[60] Soori, M., Arezoo, B., and Habibi, M., 2016, "Tool Deflection Error of Three-Axis Computer Numerical Control Milling Machines, Monitoring and Minimizing by a Virtual Machining System," ASME J. Manuf. Sci. Eng., **138**(8), p. 081005.
[61] Bosetti, P., Bort, C. M. G., and Bruschi, S., 2013, "Identification of Johnson-Cook and Tresca's Parameters for Numerical Modeling of AISI-304 Machining Processes," ASME J. Manuf. Sci. Eng., **135**(5), p. 051021.